AIChE WILEY InterScience DISCOVER SOMETHING GREAT

Biomass Gasification in a Bubbling Fluidized Bed Reactor: Experiments and Modeling

Ramin Radmanesh, Jamal Chaouki, and Christophe Guy
Dept. of Chemical Engineering, École Polytechnique, Montreal, Quebec H3C 3A7, Canada

DOI 10.1002/aic.11020
Published online October 10, 2006 in Wiley InterScience (www.interscience.wiley.com).

A model is presented for the gasification of beech wood particles in a bubbling fluidized bed gasifier (BFBG). The model encompasses the hydrodynamics of the solid and gas phases as well as the different reaction kinetics. It also accounts for the freeboard where additional homogeneous reactions take place. The influential impact of the pyrolysis step on the final composition of produced fuel gas was demonstrated by applying two different kinetic models for pyrolysis. Model results are compared with the experimental work of this study and other published results on wood gasification in BFBG. Effects of equivalence ratio (ER), steam to biomass ratio (SB), bed temperature, feed location, and mass transfer between the countercurrent regions (K_w) on the gas composition of product fuel gas are studied. The model shows good agreement with the experimental results. © 2006 American Institute of Chemical Engineers *AIChE J,* 52: 4258–4272, 2006
Keywords: gasification, pyrolysis, biomass, fluidized bed reactor, mathematical modeling, air-blown gasifiers, countercurrent back-mixing model (CCBM)

Introduction

Gasification is the thermal conversion of solid carbonaceous materials to combustible fuel gas. Coal gasification, a fairly old process, has been widely used to harness energy from coal in a more environmentally benign fashion. Biomass is indeed nothing but young coal and can be featured as an alternative to coal. Two main reasons for their boost as an alternative energy source can be recognized. First, renewable energy sources mitigate greenhouse gas emission because CO_2 emitted from thermal conversion is naturally sequestered by photosynthesis. Second, biomass use as an energy resource relieves municipal and agricultural waste management from the burden of voluminous waste.

Coal gasifiers can be converted to biomass gasifiers by certain modifications. The difference between coal and biomass, however, mostly arises from the larger amount of volatile matter in biomass, which makes it more reactive compared to coal. This necessitates the need for biomass gasification studies. Many studies on the modeling of coal gasifers, in general, and coal gasification in bubbling fluidized beds, in particular, can be found in the literature. Nevertheless, modeling biomass gasification in bubbling fluidized beds has not been amply addressed. As recently indicated by Corella et al.,[1] only a few articles on the modeling of biomass bubbling fluidized bed gasifiers (BFBGs) can be found in the literature.

In general, two different approaches can be identified in the modeling of biomass gasification in BFBGs. The first approach is a kinetic-free equilibrium calculation to estimate the final composition of product gas.[2-7] The second approach, however, is more robust and takes into account the kinetics of the reactions along with the fluidized bed hydrodynamics.[8-10] The first approach is not a dynamic modeling and does not take into account the underlying chemical and transport phenomena, particularly pyrolysis and tar formation.

Double et al.[3] classified the modeling of biomass gasification in BFBGs based on the equilibrium approach. In some studies, the whole gasification mechanism—including drying, primary and secondary pyrolysis, and other chemical reactions in the gas and the solid phases—is considered as an equilibrium stage[5,7] and, in other studies, only pyrolysis is the equilibrium stage.[11,12] Mansaray et al.[5] used an Aspen® simulator to model

Correspondence concerning this article should be addressed to J. Chaouki at jamal.chaouki@polymtl.ca.

Table 1. Beech Wood Properties

Component/Property	Weight Percentage
Proximate analysis	
Char	18
Volatile	81
Ash	0.8
Ultimate analysis	
C	48.27
H	6.36
O	45.2
N	0.14
Wood particle size, d_p	<1 mm

rice husk gasification in a BFBG with a specially designed distributor. Bilodeau et al.[11] and Sadaka et al.[12] used a semiequilibrium model in which the gases resulting from pyrolysis have been accounted for through equilibrium calculations. These models can predict the variations of temperature and gas concentration in the reactor but they lack the tar formation and its cracking.

Kinetic nonequilibrium models that couple pyrolysis and both homogeneous and heterogeneous reactions (including tar formation and cracking) with transport phenomena in fluidized beds are few. Corella et al.[1] briefly reviewed the existing models for BFBGs.

In kinetic modeling of BFBGs, one needs hydrodynamics of the bed along with the kinetics of pyrolysis and various homogeneous and heterogeneous reactions. The hydrodynamics of the fluidized bed has been well studied. Most hydrodynamic properties of fluidized beds, however, have been derived at ambient temperature. Solids mixing in the fluidized bed was studied at high temperatures in our lab using radioactive particle tracking (RPT).[13] A two-phase countercurrent back-mixing model (CCBM) was used in that study to model mixing of solid particles. Pyrolysis of beech wood was also studied at moderate heating rates of 10–50 K min^{-1}.[14]

In the present study, the experimental results of beech wood gasification in a bubbling fluidized bed are used to evaluate a model for a BFBG. The presented model unifies the two previously studied aspects of the BFBG, that is, hydrodynamics at high temperatures and pyrolysis, in a single model and evaluates the pyrolysis kinetic model derived at moderate heating rates. To underscore the effect of the pyrolysis kinetic model on overall gas composition of the product gas, the previous kinetic model is compared with the one developed by Nunn et al.[15] at very high heating rates. The model is also evaluated with other experimental data. The effect of feed location and gasifying agent are evaluated in this way.

Experimental

Beech wood particles with a maximum diameter of 1–2 mm (average < 1 mm) were used as the biomass material in this study. The chemical properties of wood particles are presented in Table 1. An atmospheric fluidized bed reactor was designed and built to carry out biomass gasification experiments. Figure 1 shows a schematic of the reactor. The reactor is made of stainless steal and withstands temperatures as high as 900°C. The bed–freeboard area and the disengagement zone have inner diameters (IDs) of 78 and 150 mm, respectively; heights of the bed–freeboard and disengagement zones are 750 and 900 mm, respectively. The reactor consists of three heating zones. The temperature in each zone can be controlled separately. These zones include the preheating zone, where the fluidizing gas enters the reactor; the bed; and the freeboard zone. Temperature in each zone was measured by means of several K-type thermocouples. The bed consisted of silica sand (Geldart B classification) particles with an average particle size of 250 μm and a solids density of 2650 kg/m^3. The minimum fluidization velocity of sand particles at ambient temperature was u_{mf} = 0.09 m/s. The temperature difference between top and bottom of the bed was not more than 10°C in different experiments, which shows a good mixing in the bed.

Sampling ports are installed at five different locations of the reactor. The isokinetic sampling of product gas at different heights of the reactor was carried out through a suitable sampling train of impingement bottles to separate tar and solid particulates from the gas. Product gases, after passing through the impingement bottles, entered the gas chromatograph (GC). The micro-GC Varian CP-4900 used in this work has a repeatability relative standard deviation (RSD) of <0.5% for propane at 1 mol %. The role of the impingement bottles is to avoid tar and particulate materials entering the GC. The tar content of produced gas was not measured because of the low range of biomass flow rate in this study and the deposition of tar materials all over the cold surfaces, which affects the accuracy and repeatability of tar measurement. The GC was equipped with a thermal conductivity detector (TCD) and two columns. Molecular-sieve and Porapak® columns were used simultaneously to separate the resulting gases. A rotameter was used in the sampling line to adjust the flow rate of the sampling gas. Beech wood particles were fed to the reactor through a screw feeder. The feeding rate of the wood during the experiments varied from 5 to 20 g/min. The wood particles in gasification experiments had essentially the same particle size as in the previous TGA/GC experiments, where the kinetics of pyrolysis was studied.[14]

The feeding point is located at the top of the bed and close to the bed surface, and thus the temperature at the feeding point is considered to be the same as the bed temperature. Air at ambient temperature was used as the gasifying agent. The flow rate of air was measured by means of a rotameter. The superficial gas velocity in the bed ranged from 0.13 to 0.30 m/s at the

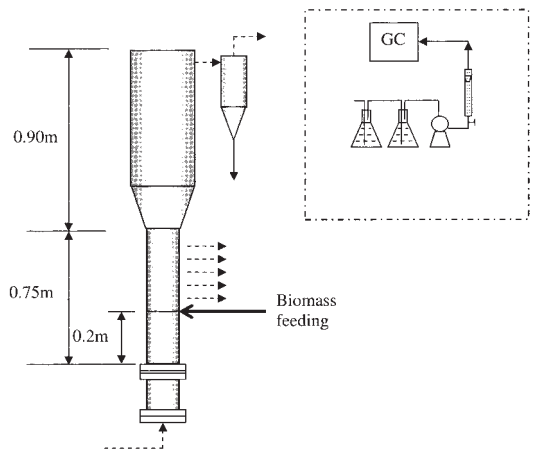

Figure 1. Bubbling fluidized bed gasifier.

bed condition (high temperature, atmospheric pressure). The reactor was operated at a bed temperature of 800°C; temperature of the freeboard was kept in the range of 700–750°C. The residence time of the gases in the freeboard was dependent on freeboard temperatures and varied from 2 to 4 s.

Model

A one-dimensional model is used to simulate the fluidized bed gasifier under isothermal conditions. The fluidized bed and, consequently, the model consisted of two parts: the fluidizing bed and freeboard. Immediately after feeding the biomass materials, because of the instantaneous decomposition of carbonaceous material, the gaseous products of pyrolysis are released in the reactor. The major products of pyrolysis are char, tar, and end-product stable gases such as CO, CO_2, CH_4, H_2, and H_2O.

The well-known two-phase model is used to describe the fluidized bed. The bed is divided into a particle-lean bubble phase surrounded by a particle-rich emulsion phase. Heterogeneous and homogeneous reactions can take place in these phases. Mass transfer occurs between the bubble and emulsion phases. Solid phase (char) is modeled by the countercurrent back-mixing (CCBM) model. The main features and assumptions of the model can be summarized as follows:

1. Pyrolysis is considered to take place instantaneously in the feeding zone of the fluid-bed gasifier. This is because solid mixing in the experimental condition of this work is much slower than pyrolysis. The reaction time constant for overall pyrolysis (Table 3) at the temperature of the reactor, which is defined as $\tau_p = 1/K_1 e^{-E/RT}$ is in fact one order of magnitude smaller than the mixing time constant, defined as $\tau_m = 1/K_w$. The ratio of τ_m/τ_p is in the range of 7–14 for different experimental conditions, which indicates that solid mixing proceeds more slowly than solid pyrolysis. In other words, wood particles undergo pyrolysis before they get a chance to mix in the fluid bed.
2. The yield of different products, including volatile products, char, and tar, is determined based on the kinetic models developed earlier.[14]
3. Carbon is assumed to be the only constituent of char.
4. The bed is under isothermal condition. This is consistent with the experimental observation during biomass gasification.
5. The composition of products calculated in the pyrolysis stage is used as the boundary condition in the following step to solve mass balance equations in the bed and freeboard.
6. The CCBM model is used to describe char particles mixing in the fluidized bed.[16] This model was applied by the authors to a fluidized bed of sand particles at high temperatures.[14] Figure 2 is a schematic representation of the CCBM model. The solid phase is where the heterogeneous reactions of char particles occur. Therefore, the reaction terms were included in the CCBM model. Parameters of the CCBM model that were calculated at high temperatures in our previous work are used in this study to describe the mixing of char particles.
7. It is assumed that char particles and their change in properties during the course of the reaction do not significantly affect the transfer coefficient between the countercurrent regions (K_w). This is because K_w is primarily affected by the dynamics and size of the bubbles and, because the total mass of char is negligible compared to that of the inert silica sand particles, the dynamics of the bed is not affected.
8. Our earlier experiments and results reveal the importance of the freeboard area where other homogeneous reactions, and especially tar cracking, take place.[17] Thus, this zone is also considered in the modeling.
9. The voidage of the dense phase throughout the bed is equal to ε_{mf}.[18]
10. The volume fraction of solids in the bubble phase is taken to be 0.005.[18]

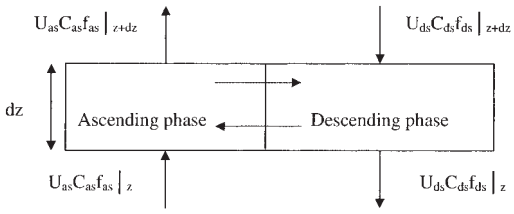

Figure 2. A demonstration of the CCBM model.

Energy balance for a single wood particle

When the solid wood particles enter the hot bed of sands, they are subject to fast pyrolysis. The rate of temperature increase in the wood particles is important in calculating the final yield of different gases. In the range of particle sizes of this study (<1 mm) the internal heat transfer limitation is negligible.[19] Moreover, the yield of the different products in pyrolysis of biomass in fluidized bed has been shown to be independent of particle size in the range of 4 μm to 2 mm.[20] This eliminates the possibility of secondary reactions between the evolving vapor products and tar with char and the consequent thermal impact (endothermic or exothermic) of those reactions on particle temperature. In this condition, the heat balance for a single particle can be expressed as follows:

$$\rho_p C_p V_p \frac{dT}{dt} = h_{conv} A (T_b - T_p) + \sigma_{rad} \varepsilon_{rad} A (T_b^4 - T_p^4) \quad (1)$$

The convection heat transfer coefficient is calculated by the Ranz–Marshall correlation reported by[18]

$$\frac{h_{conv} d_p}{k_g} = 2 + 0.6\ \mathrm{Re}^{1/2}\mathrm{Pr}^{1/3} \quad (2)$$

The effective emissivity in the condition of fluidized bed is calculated according to the correlation developed by Linjewile[21]:

$$\varepsilon_{rad} = \frac{1}{\varepsilon_p} + \frac{1}{\phi\left(\frac{1}{\varepsilon_{fb}} - 1\right)} \qquad \phi = \left(1 + n_p \frac{d_i}{d_a}\right)^2 \quad (3)$$

Table 2. Parameters Used for Energy Balance

Parameter	Value	Reference
Wood specific heat	$C_p = 1112.0 + 4.85(T - 273)$, J kg^{-1} K^{-1}	Koufopanous et al.[22]
Density of the wood	360, kg/m^3	Di Blasi[23]
ε_p for wood particles	0.95	Babu and Chaurasia[24]
Effective emissivity, ε_{fb}	0.8	Linjewile[21]
Parameter in Eq. 3, n_p	5	Linjewile[21]
Stephan–Boltzmann constant, σ	5.67×10^{-8} W m^{-2} K^{-4}	

where ε_p is the emissivity; ε_{fb} is the effective emissivity of the fluidized bed; and d_i and d_a are the diameters of the inert and active particles, respectively. Thermal properties of wood particles can be found in Table 2. The density of wood particles changes during the course of pyrolysis. The change in the density was assumed to be proportional to the loss of the volatile matter in the particle which is defined by the following:

$$\rho(t) = \rho_0\left[1 - \frac{V(t)}{V^*} X_{vm}\right] \tag{4}$$

where X_{vm} is the volatile matter of the wood particles.

Kinetic models

Pyrolysis. The biomass particles undergo pyrolysis upon their entering the fluidized bed of hot sand particles. Pyrolysis is indeed the decomposition of biomass structure resulting from heat. In gasification and pyrolysis, the final composition of product fuel gas is important. This is because the final heating value of the gaseous product depends on its composition. In pyrolysis, therefore, kinetic models for both total devolatilization, which determines the extent of produced char, and individual gas release should be taken into consideration.

The kinetic model, which is used for all the products, is a single-step first-order reaction. It can be described by the following equation:

$$\frac{dV_i}{dt} = k_{0,i}e^{-(E_{1,i}/RT_p)}(V_i^* - V_i)^n \tag{5}$$

where V_i and V_i^* are the instantaneous and total amounts, respectively, of volatile matter for the gaseous component presented as i.

Two different pyrolysis kinetic models are used in this study and their performances in the overall modeling of BFBGs are compared. The first model is based on the work done by Nunn et al.[15] on wood at high heating rates of 1000 K/s. The kinetics equation is the same as Eq. 5.

The second model is based on our previous experiments on beech wood pyrolysis at moderate heating rates. A brief description of this model is presented. The experimental results of a previous study[13] and also other pyrolysis studies[25,26] show that the final yield of each gaseous product rises by increasing heating rates. Therefore, to account for the change of gas yields with heating rates, the first-order kinetic model presented by Eq. 5 was modified in a way that V^* was a function of heating rate. This was done by using a simple first-order model that related the change in the concentration of each gas precursor in the virgin biomass (V_i^*) to heating rate. This can be described as follows:

$$\frac{dV^*}{d(1/\beta)} = -K_v V^* \qquad \text{or} \qquad V^* = V_\infty^* \exp(-K_v/\beta) \tag{6}$$

where β is the rate of temperature increase in the particle (dT_p/dt). Tables 3 and 4 tabulate the kinetic parameters calculated by Nunn et al.[15] at high heating rates and those of our previous work at moderate heating rates, respectively.

Secondary Pyrolysis or Tar Cracking. The thermal cracking of tar, also known as secondary pyrolysis, is another important step. Because more than 60% of the primary pyrolysis product accounts for tar, this step also has an important impact on the accuracy prediction of final gas composition. The tar cracking takes place in the gas phase. Boroson et al.[28] studied the homogeneous cracking of tar resulting from sweet gum hard wood and developed a first-order kinetic model. Their model was adopted by Roth et al.[29] to calculate kinetic parameters for beech wood. That model is also used in this study:

$$tar(gas) \rightarrow \upsilon_{H_2}H_2(g) + \upsilon_{CH_4}CH_4(g) + \upsilon_{CO}CO(g) + \upsilon_{CO_2}CO_2(g) + \upsilon_{tar}tar_{inert} \tag{7}$$

The stoichiometric coefficients (υ_i) are presented in Table 5. The kinetic model is as follows[27]:

$$r_{cracking} = \upsilon_i 10^{4.98}\exp\left(-\frac{93}{RT}\right)(\rho_{tar}) \tag{8}$$

Table 3. First-Order Kinetic Parameters of Primary Pyrolysis: Model 1

No.	Component	Log(k_{01}) (1/s)	E_i (kcal/mol)	V_i^* (kg/kg biomass)
1	Total devolatilization	4.53	16.5	92
	Total gas	4.53	11.8	41
2	H_2	6.7	27	2.0
3	CH_4/C_2H_4 C_2H_6/C_3H_6	3.79	16.6	3.6
4	CO	3.36	14.6	17.0
5	CO_2	3.77	14.3	6.0
6	H_2O	3.35	11.5	5.14
7	Char = 100 − (total devolatilization)			
8	Tar = (total devolatilization) − (total gas release)			

Based on the work of Nunn et al.[15] See also Hajaligol et al.[27]

Table 4. Kinetic Parameters of Gas Evolution during Primary Pyrolysis: Model 2

Total Devolatilization Parameters for Each Pseudocomponent				
No.	Component	Log(k_{01}) (1/s)	E_i (kJ/mol)	C_1
1	Cellulose	13.9	192	0.61
2	Hemicelloluse	10.2	133	0.27
3	Lignin	3.1	86	0.11

Individual Gas Kinetic Parameters							
No.	Component	Log(k_0) (1/s)	E_i (kJ/mol)	V^*_∞ (wt %)	V^*	k_v	n
1	H_2	1.7	85	1.6	—	14.5	1
2	CH_4	1.1	45	1.1	—	8.2	1
3	CO	4.8	50	7.5	—	11	3
4	CO_2	3.0	34	15	—	6.2	3
5	H_2O	13.56	149	—	4.8	—	1
6	Tar	12.0	113	—	63.8	—	1

where ρ_{tar} is the density of the tar in the gas stream and υ_i is the stoichiometric coefficient as presented in the Table 5.

Tar Combustion. Tar material, like char and other combustibles, is subject to combustion. The kinetic model of Brydon et al.[31] was used in this part for the combustion of tarry materials:

$$CH_{1.522}O_{0.0228} + 0.867O_2 \rightarrow CO + 0.761H_2O$$

$$r_8 = M_{CH} 9.2 \times 10^6 T \exp(-9650/T) \quad (9)$$

where M_{CH}, the molecular mass of tar material, =90 kg/kg mol according to Brydon et al.[31]

Homogeneous and Heterogeneous Reactions. Table 6 shows all the homogeneous and heterogeneous reactions involved in the gasification of biomass. These reactions take place after the primary pyrolysis of biomass in the bed and freeboard.

Mathematical description of the model

Fluidized Bed. The following presents the mass balance for the gas phase in the bubble and emulsion phases (Eqs. 10 and 11) and mass balance for the char particles in the ascending and descending phases (Eqs. 12 and 13):

- Bubble phase

$$-\delta_b \frac{d(\rho_g y_{i,b} u_b)}{dz} + K_{be}\rho_g(y_{i,e} - y_{i,b}) + \delta_b(1-\gamma_b)\sum_{g-g} \upsilon_{ij} R_i + \delta_b \gamma_b \sum_{g-s} \upsilon_{ij} R_i = 0 \quad (10)$$

- Emulsion phase

$$-(1-\delta_b)\varepsilon_{mf}\frac{d(\rho_g y_{i,e} u_e)}{dz} + K_{be}\rho_g(y_{i,b} - y_{i,e}) + (1-\delta_b)\varepsilon_{mf} \times \sum_{g-g} \upsilon_{ij} R_i + (1-\delta_b)(1-\varepsilon_{mf})\sum_{g-s} \upsilon_{ij} R_i = 0 \quad (11)$$

The gas density is calculated assuming an ideal gas behavior:

$$\rho_g = \frac{P}{RT}\left(\sum y_{i,g} M_i\right) \quad (12)$$

- Char balance in the ascending phase

$$\omega_{as,0}\frac{dX_{as}}{dz} + K_w(C_{ds,c} - C_{as,c})Af_{as} + Af_{as}\sum_{g-s} \upsilon_{i,c} R_i = 0 \quad (13)$$

- Char balance in the descending phase

$$-\omega_{ds,0}\frac{dX_{ds}}{dz} + K_w(C_{as,c} - C_{ds,c})Af_{as} + A(1-f_{as})\sum_{g-s} \upsilon_{i,c} R_i = 0 \quad (14)$$

- Char concentration in countercurrent regions

$$C_{as,c} = \frac{\omega_{as,0}}{U_{as} f_{as} A}(1 - X_{as})$$

$$C_{ds,c} = \frac{\omega_{ds,0}}{U_{ds} f_{ds} A}(1 - X_{ds}) \quad (15)$$

Equations 10 and 11 give the gas concentration profile in the bed, whereas Eqs. 12 and 13 provide the char conversion profile in the bed, which is needed for char reaction kinetics. Thus, these equations must be solved simultaneously for all the gas species to obtain produced gas compositions and yields in the bed. The boundary condition for these equations is pro-

Table 5. Stoichiometric Coefficients for Tar Cracking

Component	υ_i
H_2	0.0173316
CH_4	0.0884052
CO	0.563316
CO_2	0.1109316
Secondary tar	0.22

After Wurzenberger et al.[30]

Table 6. List of Heterogeneous and Homogeneous Reactions Involved in Gasifiers

No.	Chemical Reaction	Kinetic	Reference
R1	$\lambda C + O2 \rightarrow 2(\lambda - 1)CO + (2 - \lambda)CO2$	$r_1 = \frac{dX}{dt} = 1.5 \times 10^6 \exp\left(\frac{-13.078}{T_{par}}\right) p_{O_2}(1 - X_c)^{1.2}$ $\lambda = 3 \times 10^8 \exp\left(\frac{-30178}{T_{par}}\right)$	Wurzenberger et al.[30]
R2	$C + H_2O \rightarrow CO + H_2$	$r_2 = \frac{k_2 p_{H_2O}}{1 + k_3 P_{H_2O} + k_4 p_{H_2}}$ 1/s $k_2 = 4.93 \times 10^3 \exp\left(\frac{-18522}{T_{par}}\right)$ $k_3 = 1.11 \times 10 \exp\left(\frac{-3548}{T_{par}}\right)$ $k_4 = 1.53 \times 10^{-9} \exp\left(\frac{25161}{T_{par}}\right)$	Wurzenberger et al.[30]
R3	$C + CO_2 \rightarrow 2CO$	$r_3 = 2 \times 10^{-8} exp(-360{,}065/T_{par})[CO_2]$ kmol m^{-3} h^{-1}	Biba et al.[32]
R4	$CO + 1/2O_2 \rightarrow CO_2$	$r_5 = 10^{17.6} \exp(-20{,}000/T_g)[CO]^{0.25}[H_2O]^{0.5}$ kmol m^{-3} s^{-1}	Bryden and Ragland[31]
R5	$H_2 + 1/2O_2 \leftrightarrow H_2O$	$r_6 = 2.19 \times 10^{15} \exp(-13{,}127/T_g)[H_2][O_2]$	Wurzenberger et al.[30]
R6	$CH_4 + 2O_2 \rightarrow CO_2 + 2H_2O$	$r_7 = 1.58 \times 10^{16} \exp(-24{,}343/T_g)[CH_4]^{0.7}[O_2]^{0.8}$	Wurzenberger et al.[30]
R7	$CO + H_2O \rightarrow H_2 + CO_2$	$r_8 = 2.7 \times 10^3 \exp\left(-\frac{1510}{R_g}\right)\left[[CO][H_2O] - \left(\frac{[CO_2][H_2]}{K^*}\right)\right]$ $K^* = 0.0265 \exp\left(\frac{3968}{T_g}\right)$	Biba et al.[32]
R8	Tar cracking reaction	$r_{cracking} = \upsilon_i 10^{4.98} \exp\left(-\frac{93}{RT}\right)(\rho_{tar})$ kg m^{-3} s^{-1}	Hajaligol et al.[27]
R9	Tar combustion	$r_8 = M_{CH}\, 9.2 \times 10^6 T \exp(-9650/T)$ kg m^{-3} s^{-1}	Bryden and Ragland[31]

vided by the fluidizing gas composition at the distributor level and pyrolysis model at the feeding level.

Table 7 lists the hydrodynamic parameters used in the preceding equations along with the necessary correlations to estimate these parameters. The velocities of the ascending and descending phases are derived from the previous hydrodynamic studies in our lab.[14] In the same study, it was shown that the K_w value given by Hoffmann et al.[35] was in a good agreement with our experimental data at high temperatures. Therefore, this correlation, as shown in Table 7, is used herein to calculate the transfer coefficient between the countercurrent regions. Table 7 also represents another correlation for K_w (that is, the Kocatulum correlation[36]), which results in a larger deviation with our experimental data on the mixing study at high temperatures. This correlation is merely used to evaluate the effect of K_w on model prediction. It is assumed that the K_w calculated for the sand particles can be used for the char particles. This is justifiable by considering that K_w is more dependent on the bubble diameter.

Freeboard. The freeboard region above the bed provides a space not only for disengagement of solids but also further reactions. The gas that leaves the bed enters the freeboard section that behaves as a second reactor in series with the fluidized bed. Homogeneous and heterogeneous reactions as well as tar cracking continue in the freeboard region. Models to predict the entrainment of particles from the bed are available in the literature.[37] As was mentioned earlier, biomass materials contain a low proportion of char and a large proportion of volatile matter (see Table 1). As a result, it is assumed that the char particles are consumed in the bed and thus entrainment of the char is negligible.

A plug-flow model in this condition of low solids concentration and gas velocity is reasonable. Tar cracking and water–gas shift reactions are the most important reactions that take place in this region. Depending on the biomass feeding location, other combustion reactions may also occur in the freeboard. The mass balance for each species in this region is given by the following differential equation:

$$\frac{d(u_f \rho_{i,g})}{dz} = \sum_{g-g} \upsilon_{ij} R_i \tag{16}$$

where u_f is the gas velocity in the freeboard, ρ_i is the density of different gas species, and R_i is the gas-phase reaction rate determined by the kinetics presented in Table 6.

Results and Discussion

Model comparison with experiments

The experimental data in this study were collected in a fluidized bed gasifier with a top feeding of biomass close to the bed surface (see Figure 1). As was shown by Corella et al.,[38] the location of biomass feeding (from the top or bottom of the bed) affects the distribution of gaseous products. In feeding from the bottom, pyrolysis products pass through the bed and thus there is a better mixing of the product gases resulting from pyrolysis. Moreover, tar, in this case, is more prone to crack

Table 7. Hydrodynamic Parameters Used in This Study

Parameter	Correlation	Reference
Minimum fluidization velocity	$\mathrm{Re}_{p,mf} = [(27.2)^2 + 0.0408\ Ar]^{0.5} - 27.2$	Grace[33]
Bubble diameter	$d_b = d_{bm} + (d_{b0} - d_{bm})e^{-0.3Z/d_t}$ $d_{bm} = 0.65[\pi/4d_t^2(u_0 - u_{mf})]^{0.4}$ $d_{b0} = 1.3/g^{0.2}(u_0 - u_{mf}/N_{or})^{0.4}$	Kunii and Levenspiel[18]
Bubble velocity	$u_b = u_0 - u_{mf} + u_{br}$ $u_{br} = 0.711(gd_b)^{0.5}$	Davidson and Harrison[34]
Bubble fraction	$\delta_b = \dfrac{u_0 - u_{mf}}{u_b - u_{mf}}$	Kunii and Levenspiel[18]
Bubble-cloud transfer coefficient	$K_{bc} = 4.5\left(\dfrac{u_{mf}}{d_b}\right) + \dfrac{5.85D^{0.5}g^{0.25}}{d_b^{1.25}}$	Kunii and Levenspiel[18]
Cloud-emulsion transfer coefficient	$K_{ce} = 6.77\left(\dfrac{D\varepsilon_{mf}u_{br}}{d_b^3}\right)^{0.5}$	Kunii and Levenspiel[18]
Bubble-emulsion transfer coefficient	$\dfrac{1}{K_{be}} = \dfrac{1}{K_{bc}} + \dfrac{1}{K_{ce}}$	Kunii and Levenspiel[18]
f_{as}	$0.45 < f_{as} < 0.5$	Radmanesh et al.[14]
U_{as} (m/s)	$0.03 < U_{as} < 0.07$	Radmanesh et al.[14]
U_{ds} (m/s)	$0.05 < U_{ds} < 0.07$	Radmanesh et al.[14]
Wake exchange coefficient	$K_w = \dfrac{0.081}{2\varepsilon_{mf}d_b}$	Hoffman et al.[35]
Wake exchange coefficient	$K_w = 0.807\dfrac{u_b}{d_b}$	Kocatulum et al.[36]

and the yield of stable gases increases as a result. Feeding into a bed of sand at a temperature of 800°C, however, is not always an easy task. Furthermore, as shown in this work, feeding into the bottom of the bed, where oxygen still exists, leads to the combustion of some combustible gases and may even reduce the final heating value of product fuel gas. In feeding from the top, the gas phase, including the tar, does not pass through the hot bed. The char particles in the bed undergo combustion and gasification (R1–R3). The resulting gases from these reactions (CO and CO_2) mix with the pyrolysis gas, which are calculated from the pyrolysis model. Homogeneous reactions, especially tar cracking and shift reactions, continue in the freeboard area of the reactor. The high temperature of the freeboard in these experiments favors the tar cracking reaction in this zone. However, depending on the flow rate of gasifying agent (that is, air) and whether all the oxygen has been consumed in the bed, some gas-phase combustion may also occur in this section.

Several experiments were performed with beech wood in a bubbling fluidized bed reactor. The experiments were done at different equivalence ratios (ERs). ER is an important parameter in the air-blown biomass gasification.[39,40] It is defined as the air-to-fuel mass flow ratio used in the experiment divided by the air-to-fuel mass flow ratio required for a complete combustion. Table 8 summarizes the operating conditions in each gasification experiment and the resulting gas-phase product composition.

The profile of each gas along the height of the reactor is calculated by solving Eqs. 9–14 in the bed and freeboard. Boundary conditions for the balance equations in the bed are given by the pyrolysis kinetic model, which gives the compo-

Table 8. Experimental Operating Condition and Product Gas Composition in Dry Basis

						Gas Composition at Exit (Dry Basis %)				
Run	T_{bed} (°C)	T_f (°C)	m_b (g/min)	u^* (m/s)	ER	H_2	CH_4	CO	CO_2	N_2
1	805	750	12	0.21	0.32	9.2	2.5	16.2	12.7	59.6
2	800	760	14	0.17	0.23	11.5	4.1	20.5	12.9	50
3	805	755	13	0.38	0.48	5.9	0.60	9.2	12.8	71
4	800	740	18	0.13	0.13	14.3	4.5	27.0	8.60	56
5	815	740	15	0.17	0.22	14.7	4.4	20.2	11.8	49
6	800	730	16	0.21	0.24	11.7	3.3	20	12.4	53
7	800	740	5.5	0.17	0.66	4.8	0.93	11	14	69

Air velocity at the bed condition.

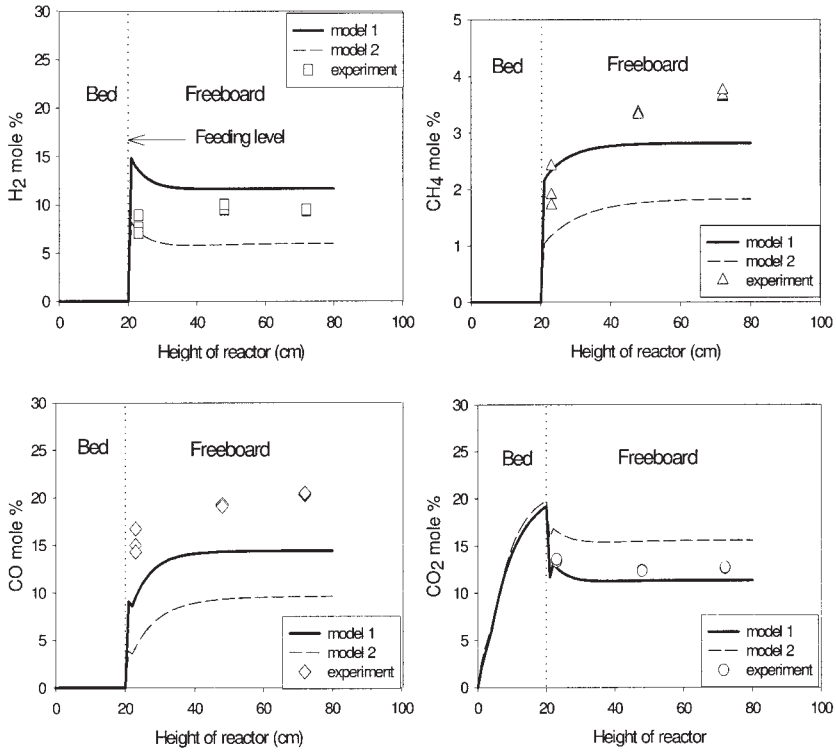

Figure 3. Concentration profiles of the gases along the reactor height.

Comparison of two pyrolysis kinetic models. $T_{bed} = 800°C$, $T_f = 740°C$, and ER = 0.32.

sition of the gases, tar, and char; these gas compositions constitute a boundary condition for the gasification in the bed. Two kinetic models, presented earlier, are used in this part. Gas composition calculated at $z = H_{bed}$ provides the boundary condition for the freeboard section.

Figure 3 portrays the concentration profile of the four major gases as a function of reactor height resulting from the first and second pyrolysis kinetic models (Tables 2 and 3) at a bed temperature of $T = 800°C$ and ER = 0.32. It also compares two models with the experimental results of beech wood gasification at the same operating conditions. This figure demonstrates the importance of the pyrolysis step in final gas composition. As it shows, the first pyrolysis kinetic model, which was derived at higher heating rates, can satisfactorily predict product gas composition. This, apparently, suggests a change in pyrolysis mechanism at very high heating rates, which forces a new distribution in the final product gas concentration. Therefore, the kinetic model derived at higher heating rates estimates the final gas composition relatively better than the one derived at lower heating rates.

The dotted lines in Figure 3 represent the feeding location, which is at top of the bed at height of $z = 0.20$ m. As a result of the sudden pyrolysis of wood in the feeding area, abrupt changes in the gas concentrations can be observed at that height. The model is able to predict the composition of product fuel gas. Figure 4 shows the same profile for the first pyrolysis kinetic model but at ER = 0.13. Oxygen concentration is also shown in this figure. The concentration of oxygen drops from the bottom to the top of the bed and it almost disappears at the feeding point.

Figure 5a compares total gas yield predicted by two pyrolysis kinetic models with the experiments at different ER values. The gas yield is defined as the total mass of gas produced at the exit of the reactor (top of the freeboard) divided by the mass of consumed biomass. The two models result in very close prediction of total yields. However, the distribution of gases, which is a determining factor in heating value of the gas product, is entirely different. The higher heating value (HHV) of the dry gas at the standard state can be estimated by the following equation[7]:

$$\text{HHV} = (12.75[\text{H}_2] + 12.63[\text{CO}] + 39.82[\text{CH}_4])/100 \text{ MJ/Nm}^3 \quad (17)$$

This equation was derived based on the heat of combustion of different gases. The gas concentration in Eq. 17 is in mol %. Figure 5b shows the HHV estimated by Eq. 17 for the product gas as a function of ER. The difference in the product distribution arises mainly from the prediction of CO and CO_2, where the second model always overestimates the yield of CO_2 and underestimates that of CO. Thus, the heating value of the gas predicted by the first model is higher than that by the second model and experimental data. Figure 5a also demonstrates an increase in the total gas yield by increasing ER. This is in accord with previous studies.[40,41] Both models are able to predict the gas yield increase with ER. The heating value of the product gas, however, decreases by increasing ER because of the larger contribution of CO_2 in the yield of gaseous product.[10] This, in turn, is a result of a higher contribution of combustion (of char, tar, and other combustible gases) and a lesser contribution of gasification in the overall reactions with increasing

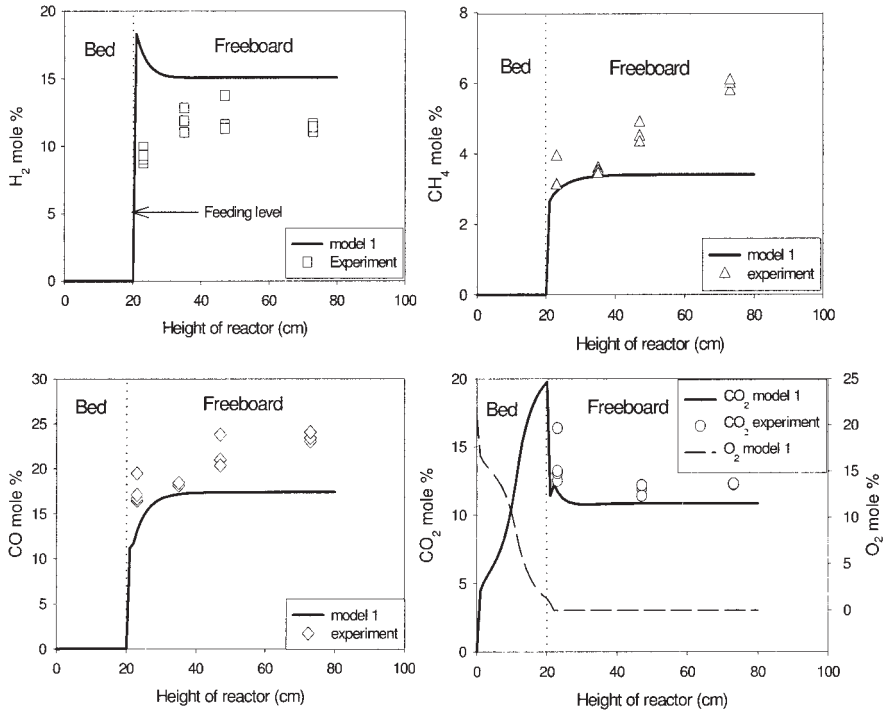

Figure 4. Concentration profile of the gases along the reactor height.

T_{bed} = 800°C, T_f = 740°C, and ER = 0.13.

ER. The dilution of the product gas by N_2 also contributes to the lower HHV at higher ER.

The effect of ER on dry gas composition and yield of each individual gas are presented in Figures 6 and 7. The lines in these figures represent the model resulting from the first pyrolysis kinetic model[15] and symbols are the experimental points. An increase in ER brings about a decrease in the concentration of H_2 and CO and a substantial increase in CO_2 concentration in dry gas product. This is because of the increasing role of the char combustion in the bed compared to its gasification reaction, which results in lower concentration of combustible gases and higher CO_2. These results are in agreement with the previous result published by Gil et al.[41] Lim et al.[7] reported the same trend of gas composition changes with air ratio (ratio of actual air to stoichiometric required air) in a circulating fluidized bed.

The model can also predict the amount of tar content in the produced gas. The effect of ER on tar content predicted by the model is presented in Figure 8. As has been well established, an increase in ER promotes combustion of produced tar and thus reduces the tar content in the exit gas. The amount of tar presented in this figure is the summation of initial tar and final inert tar in the kinetics of tar cracking (Eq. 7). Narvaez et al.[40] reported a lower tar amount in the range of 0.010–0.025 kg/Nm^3, compared to 0.04–0.1 kg/Nm^3 presented in Figure 8, in their air-blown fluidized bed gasifier with bottom feeding of biomass. Their experimental data clearly show, however, the same trend in the tar content with ER. The main reason for the higher tar amount predicted by the model compared to the experimental data of Narvaez et al.[40] lies in the feeding location. A greater degree of combustion of tar material takes place

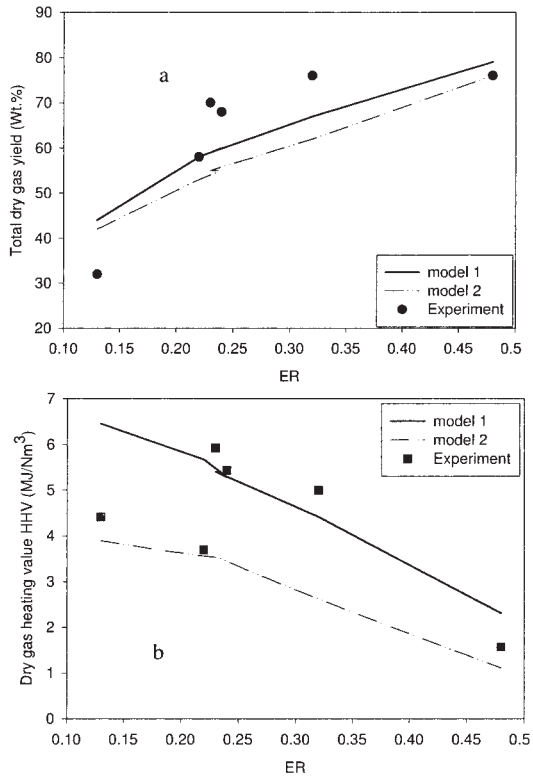

Figure 5. Total dry gas yield [kg of produced gas/kg of dry, ash-free (daf) biomass] and heating value of the dry gas (MJ/Nm^3) at the exit of the reactor.

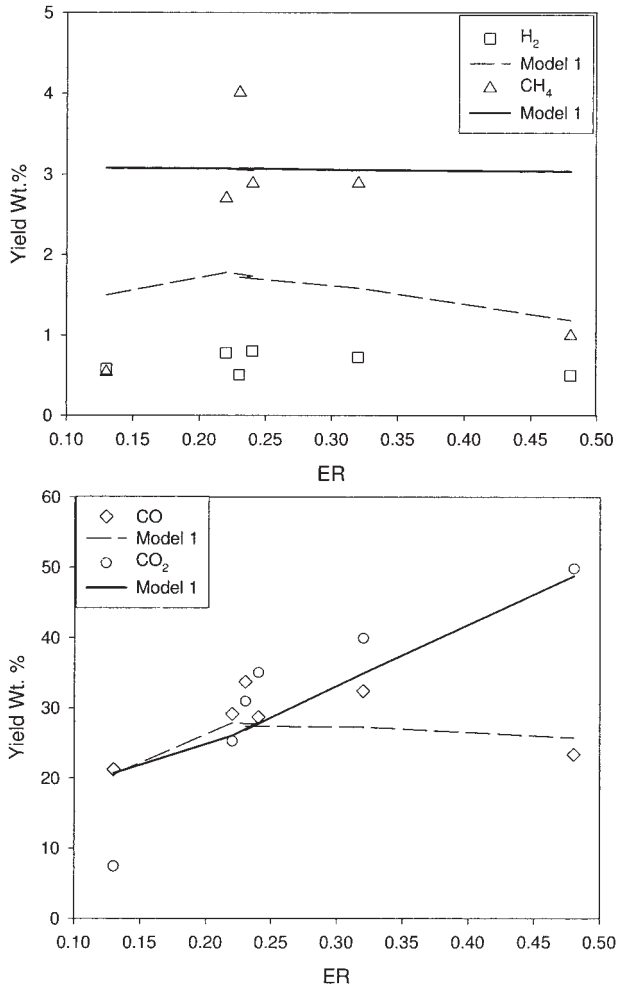

Figure 6. Individual dry gas yield at different ER values and T_{bed} = 800°C.

Comparison of model with experiments (top feeding).

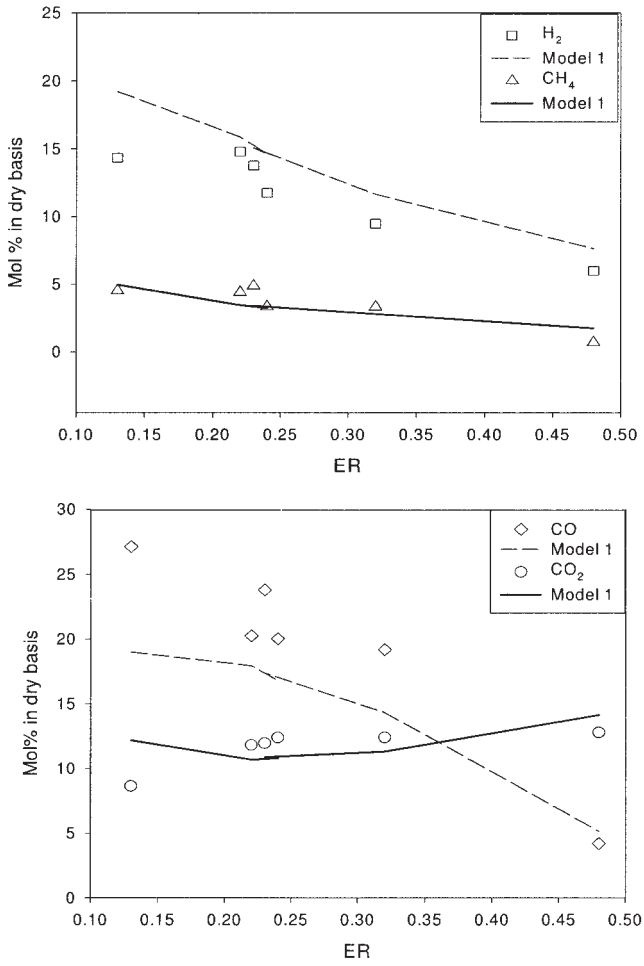

Figure 7. Concentration of individual gases in dry basis at different ER values and T_{bed} = 800°C.

Comparison of the model with experiments (top feeding).

in the bottom feeding where biomass is directly fed to a rich oxygen zone close to the distributor.

Sensitivity analysis

The model shows a good agreement with the experimental work of this study. The model also enables investigators to study the influence of operating and hydrodynamics variables. The variables selected for the analysis are feeding point of the biomass (that is, top and bottom feeding), ER, bed temperature, type of gasifying agent, and K_w or the transfer coefficient between the countercurrent regions. Model predictions in each case are compared with other experimental data that was carried out at the bubbling fluidized bed with different diameters. The model is also extrapolated to higher flow rate of gasifying agent and the effect of superficial gas velocity is considered on the heating value of the gaseous product.

Air-blown BFBG

Effect of Feed Location. Corella and coworkers have done extensive experimental work on biomass gasification in bubbling fluidized bed reactors.[40-43] Because the size of the fluidized bed used in this study is very close to that used by these authors, their experimental results are compared to the model. This also allows an investigation of the effect of feeding

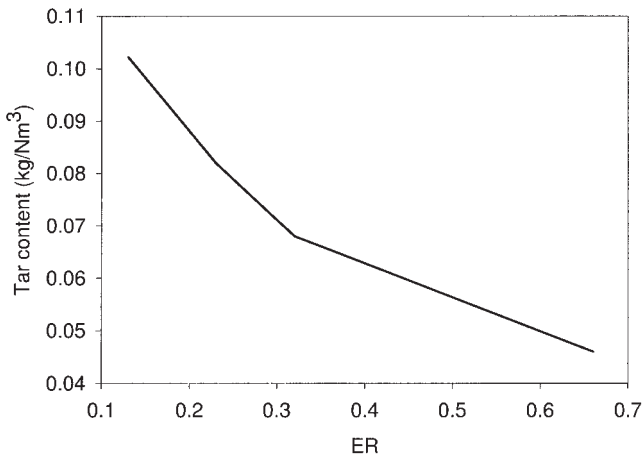

Figure 8. Tar content in the exit gas from the gasifier under normal conditions.

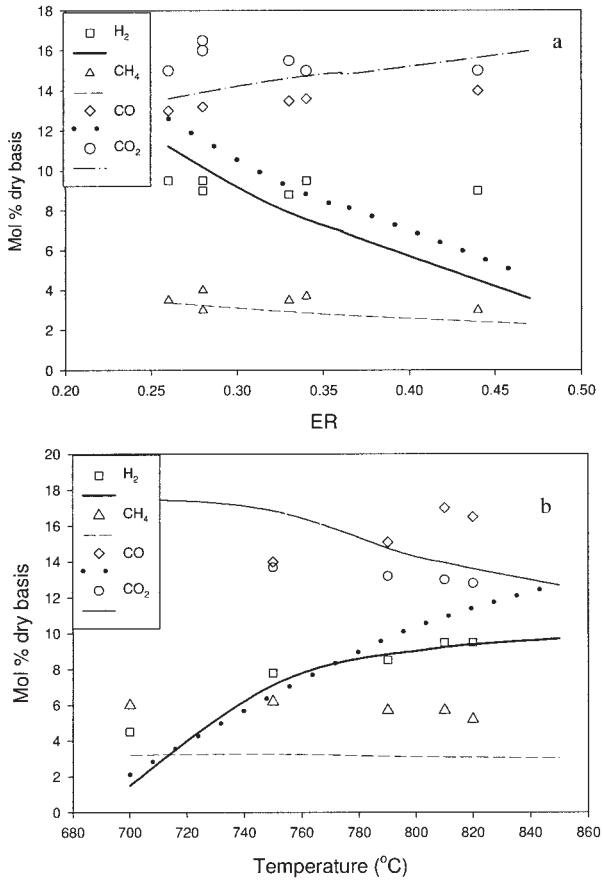

Figure 9. Model vs. experiments[40] in air-blown BFBG with bottom feeding.

(a) Effect of ER on concentration at $T = 800°C$. (b) Effect of temperature on concentration at ER = 0.3.

location on gas compositions. Narvaez et al.[40] studied air gasification of pine sawdust in a bubbling fluidized bed of 0.06 m ID. Contrary to our experimental work, the feeding of wood particles in their experiments takes place at the bottom of bed (that is, 0.05 m above the distributor). The model was adapted to a bottom feeding of wood particles. The superficial gas velocities in both experiments are almost in the same ranges [$u = (2–3) \times u_{mf}$]. Therefore, the same range of parameters for char mixing in the bed was assumed to be applicable here as well. Moreover, back-mixing of the product gases has only minor importance because of the low superficial gas velocities.

Figure 9 compares the model results with the experimental work of Narvaez et al.[40] Figure 9a shows the effect of ER and bed temperature on the dry gas composition of the product fuel gas. The effect of ER on gas concentrations is almost the same as the top feeding presented in Figure 7. Figure 9a shows a disagreement between the model and experimental data of Narvaez et al.[40] with respect to CO and H_2 concentration. Higher ER values result in greater combustion of char and combustible gases and thus one expects a drop in the concentration of CO and H_2 at higher ER. The lower heating value (LHV) at higher ER reported by Narvaez et al.[40] and other researchers is also another evidence for this trend. Although Narvaez et al.[40] mentioned in their article: "In the interval studied for ER (from 0.20 to 0.45), on increasing ER, the amount of fuel gases (H_2, CO, CH_4, and C_2H_2) decreases . . .", their experimental data, also reflected in Figure 9a, do not demonstrate that. The effect of bed temperature at a constant value of ER = 0.3 is presented in Figure 9b. High temperature greatly favors the gasification reactions (R2 and R3 in Table 6) and, as a result of that, the heating value of the product gas increases. This is reflected in Figure 9b where the concentrations of H_2 and CO substantially increased from 700 to 800°C.

Both model and experimental data show a difference on the distribution of product gases between top and bottom feeding. In bottom feeding, the product gases from the pyrolysis step enter directly into the region of the bed where the concentration of oxygen is high. As a result, light gases, such as H_2 and CO, as well as tar, are prone to combustion in the bed. In top feeding, on the other hand, the gas product from the pyrolysis step enters in a region that has already become depleted of oxygen, mainly through the char combustion in the bed. Consequently, concentrations of H_2 and CO are higher in the top feeding. This is also reflected in Figures 10a and 10b, which show the effect of temperature and ER on HHV of the product gas. A comparison between this figure and Figure 5b shows a lower heat content of the gaseous product in bottom feeding. The HHV of the product gas resulting from top feeding, however, is disfavored by the higher quantity of tar, which is less prone to cracking and combustion in top feeding.

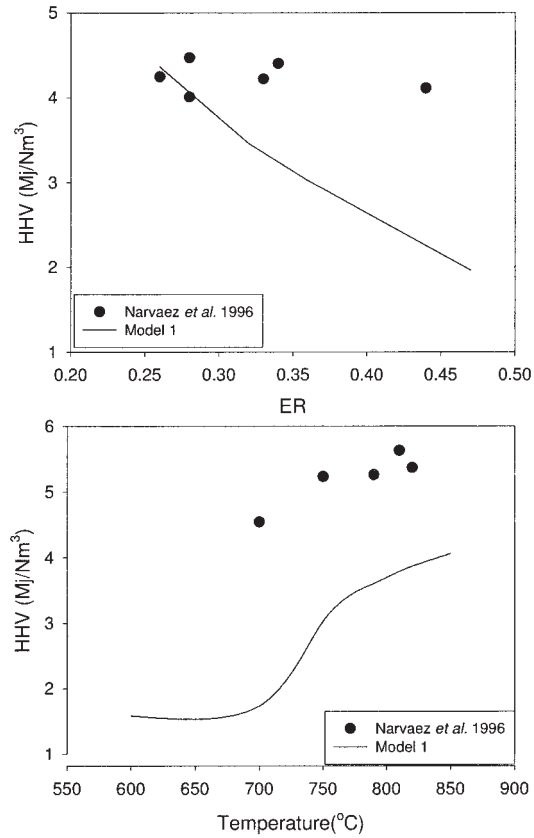

Figure 10. Higher heating value of gas at different ER values and bed temperatures.

Lines represent the model and symbols represent the experimental work.[40]

Table 9. Gasification Condition for Extrapolation of the Model*

Air Velocity (m/s)	ER	m_b (g/min)	u_b (m/s)	K_w (s^{-1})
0.29	0.25	23	0.4	0.64
0.38	0.25	30	0.45	0.85
0.53	0.25	42	0.56	0.86
0.76	0.25	60	0.73	1.2

Conditions: T_{bed} = 800°C, T_f = 540°C, bottom feeding.

Effect of Gas Velocity. The model is also extrapolated to higher superficial gas velocities. Table 9 presents gas velocities and other corresponding parameters used in the extrapolation. The bubble velocity and K_w presented in this table are those that were based on the RPT measurements at elevated temperatures. The extrapolation is carried out in a reactor with the same size and solid particles as in this study (see Figure 1). Changes on the superficial gas velocity have an impact on the hydrodynamics of the bed. Hydrodynamic changes take place mainly by changing bubble diameter and velocity. It also affects the residence time of the gas phase and, consequently, fuel gas distribution. Figure 11 shows the effect of superficial gas velocity on the fuel gas composition at two different ER values. Concentrations of H_2 and CH_4 drop by increasing air superficial velocity, resulting in a slightly lower HHV value by increasing gas velocity. The flow rate of gas that flows in the bubble phase is proportional to $u - u_{mf}$. At ER = 0.35, by increasing gas velocity more gas flows in the bubble phase and, consequently, more oxygen is available in the bubble phase. As a result, more gases are prone to combustion in this phase. Because the combustion of H_2 is very rapid compared to that of the others, a larger reduction in concentration of this gas can be observed in the product gas. Nevertheless, concentrations of CH_4 and CO also drop initially, causing an increase in CO_2 concentration at ER = 0.35. The latter drop in CO_2 concentration is likely the result of a dilution effect of N_2 at higher air mass flow. A similar trend is observed at higher ER values. A value of ER = 0.25, however, is a turning point, where the amount of oxygen in comparison to biomass is low to the point that almost all oxygen content is indeed consumed by the fast char oxidation reaction. Therefore, the concentra-

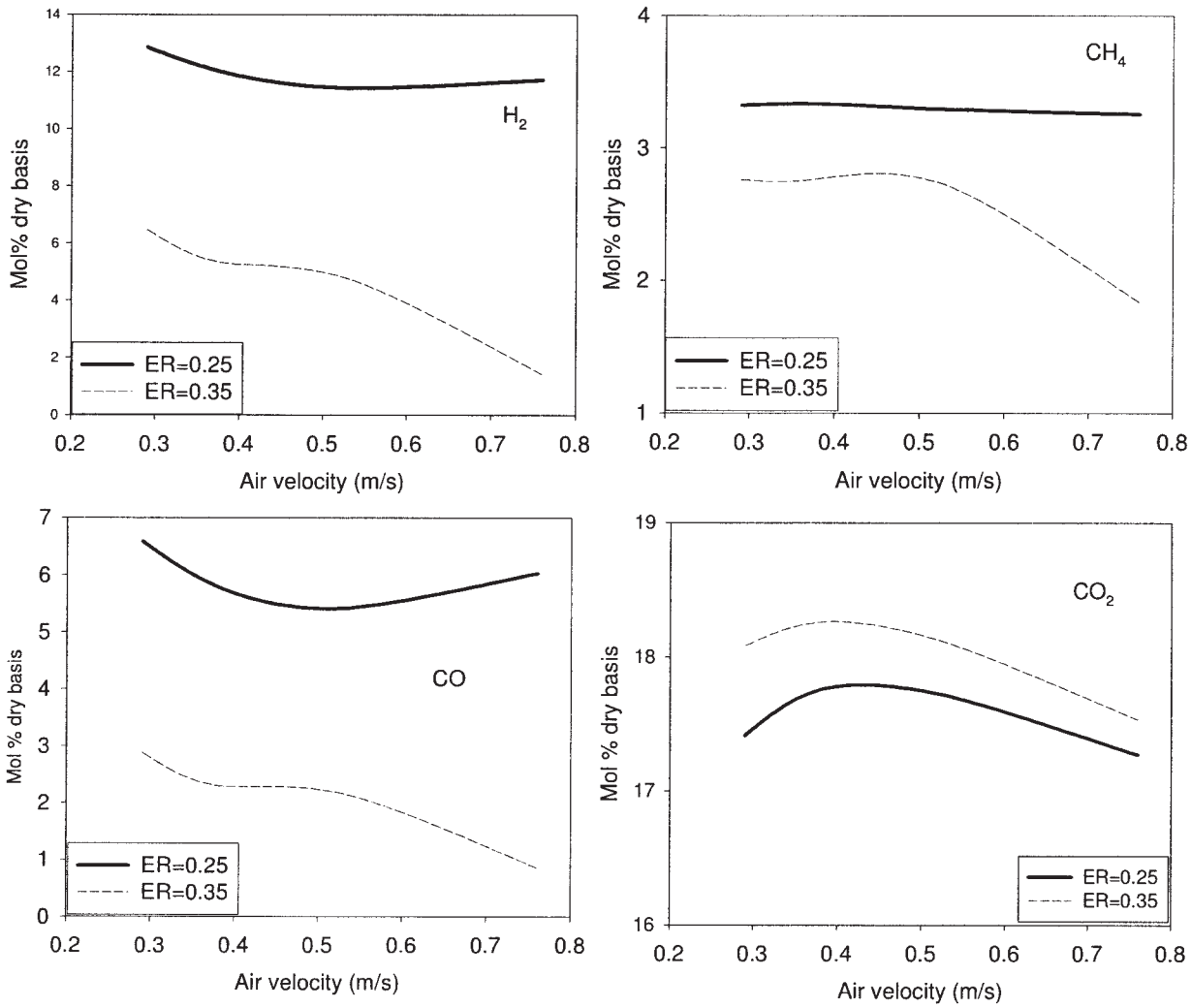

Figure 11. Gas composition vs. air superficial velocity at two different ER values.

Extrapolation of the model to higher gas velocities. T_{bed} = 800°C, T_f = 540°C.

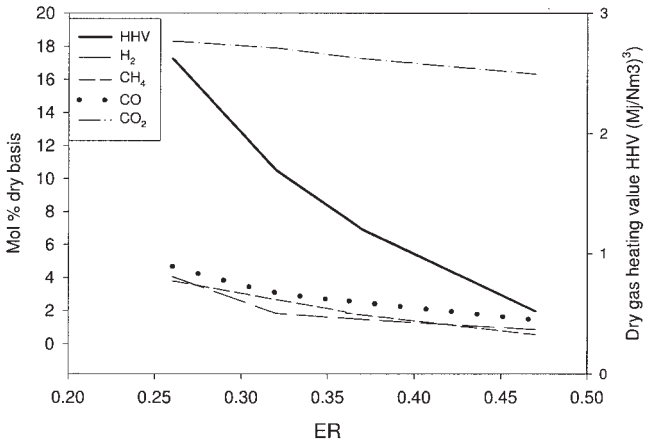

Figure 12. Gas composition and heating value of the product gas predicted by the model using a K_w given by Kocatulum et al.[36]

tions of combustible gases do not drop as significantly as at ER = 0.35.

Effect of K_w. In our previous study, the transfer coefficient between the countercurrent regions (K_w) was found to be in the range of 0.6–1.7 s^{-1} for different superficial gas velocities and bed temperatures.[14] Among all the correlations for K_w, the one given by Hoffmann et al.[35] shows a better agreement with the experimental data at high temperatures. All other correlations, including the one given by Kocatulum et al.,[36] overestimate the value of K_w.

To investigate the effect of K_w on the final composition and heating value of product gas, this correlation, as presented in Table 7, is selected. The model was solved for an air-blown gasifier with a bottom-feeding condition using the new value of K_w. Figure 12 presents the simulation results at a bed temperature of $T = 800$°C and different ER values using a K_w value given by Kocatulum's correlation. The experimental conditions are the same as those presented by Narvaez et al.[40] The K_w calculated by Kocatulum's correlation in this condition is $K_w = 5\ s^{-1}$. As Figure 12 shows, the heating value of the product gas is lower than the value based on K_w given by Hoffmann et al.[35]and experimental data of biomass gasification in a bubbling fluidized bed given by Narveaz et al.[40] (see, for example, Figure 10). This arises from the lower concentration of H_2 and higher concentration of CO_2 in the product gas. The competitive fast combustions of char and H_2 in solid and gas phases are affected by the hydrodynamics of the bed. A larger value of K_w promotes radial mixing in the solid phase but at the same time decreases the contribution of oxygen consumption through char combustion reaction, which results in a higher contribution for the H_2 combustion. Interestingly, the agreement between simulation results and experimental data is more satisfactory when using a K_w value close to the calculated range in solids mixing study at high temperatures.[14] This reveals the sensitivity of the model to the transfer coefficient between the countercurrent regions.

Steam-blown BFBG: effect of gasifying agent

In this stage, the BFBG model is applied to steam gasification of wood. The same strategy, as was presented for air-blown gasification without any adjustable parameters, is used for steam-blown gasification in this section. Experimental results of Herguido et al.[43] were carried out in a 0.15 m ID fluidized bed with bottom feeding. Figure 13 compares their experimental results for steam gasification of sawdust with the model. Figures 13a and 13b show the effect of steam to biomass mass ratio (SB) and bed temperature on the gas composition of the product gas, respectively. Unlike air gasification where the product gas is rich in CO_2 and CO, steam gasification results in H_2-rich gas. The model is capable of predicting the composition of the hydrogen in the final product gas.

Concentrations of both H_2 and CO_2 increase by increasing SB. This can be explained by the shift reaction, where the higher water concentration favors the production of CO_2 and H_2. Gil et al.[41] reported the same trend in concentration of gases in steam gasification of wood in BFBG. It is worth noting that biomass gasification using steam as the only gasifying agent does not correspond to industrial reality because of its lack of autothermicity. In reality, it is always necessary to use some air to provide the required energy for the endothermic reactions involved in steam gasification.

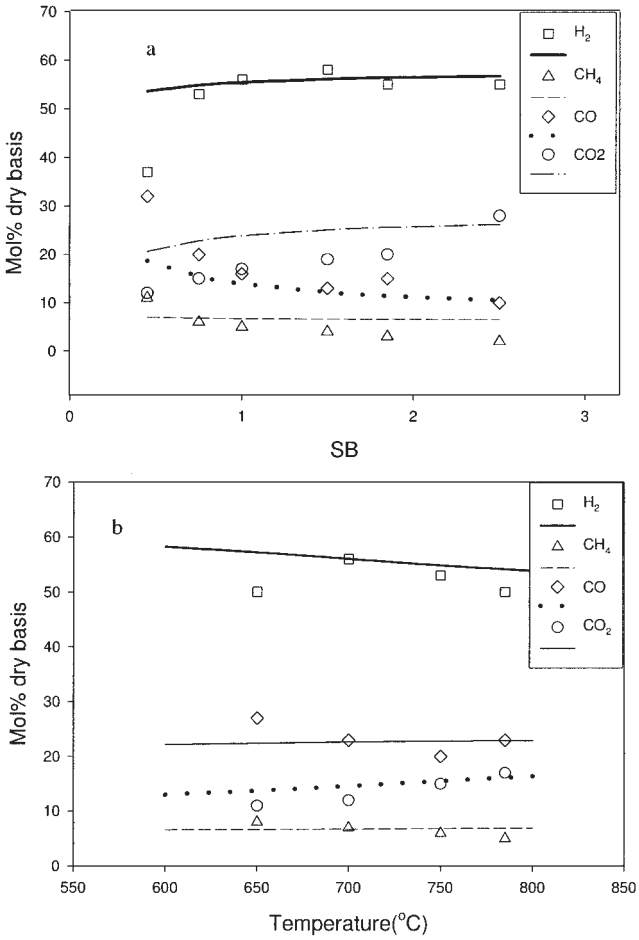

Figure 13. Model vs. experiments[43] in steam-blown BFBG with bottom feeding.

(a) Effect of SB on concentration at $T = 750$°C. (b) Effect of temperature on concentration at SB = 0.75.

Conclusions

A model was developed for biomass gasification in a bubbling fluidized bed reactor. The model takes into account the pyrolysis and various heterogeneous and homogeneous reaction kinetics as well as the hydrodynamics of the bed and freeboard. The model consists of no adjustable parameters.

A two-phase model was used to describe the gas phase in the bed, whereas a CCBM model was applied for the char mixing in the bed. It was shown that pyrolysis is an important step in the overall gasification model that can determine the distribution of products and thus the heating value of product fuel gas. Better results were obtained when using the pyrolysis model developed by Nunn et al.,[15] which was developed at higher heating rates. The gasification models, developed based on the first and second pyrolysis kinetic models, were both able to predict the variation of total gas yield with ER. However, the first kinetic model could more satisfactorily follow the distribution of gases and thus the heating value of the product fuel gas. The BFBG model also showed good agreement with experiments on steam gasification of wood, whereby concentrations of SB, H_2, and CO_2 rise and that of CO drops.

Notation

C_i = contribution coefficient of each pseudo component in biomass (see Table 4)
C_p = heat capacity, J kg^{-1} K^{-1}
d = diameter, m
E = activation energy, kJ/mol
h_{conv} = convective heat transfer coefficient, W m^{-2} K^{-1}
K_g = thermal conductivity of gas, W m^{-1} K^{-1}
$k_{0,i}$ = frequency factor for component i, 1/s
K = transfer coefficient, 1/s
M_i = molecular weight of component i, kg/kmol
n_p = parameter in Eq. 3
R_i = rate of reaction for component i
Re = Reynolds number
Pr = Prandtl number
T_{bed} = bed temperature, K
T_p = particle temperature, K
u = gas velocity, m/s
U = countercurrent regions, m/s
V_i = release volatile matter, wt %
V_i^* = ultimate final yield for component i in pyrolysis
X = conversion of char
X_{vm} = volatile content in the wood, wt %
y_i = weight fraction of component i in the gas
z = height of the freeboard, m

Subscripts

as = ascending phase
b = bubble
bc = bubble-cloud
be = bubble-emulsion
c = char
ds = descending phase
f = freeboard
i = gaseous components in the product gas j
j = reaction index
p = particle
w = wake

Greek letters

δ_b = fraction of bed in bubble
γ_b = fraction of solid in bubble, m^3/m^3
ε = emissivity coefficient
ε_{mf} = porosity at minimum fluidization velocity, m/s
ϕ = parameter in Eq. 3
ρ_i = density of component i, kg/m^3
τ = characteristic time
υ_i = stoichiometric coefficient of component i

Literature Cited

1. Corella J, Sanz A. Modeling circulating fluidized bed biomass gasifiers. A pseudo-rigorous model for stationary state. *Fuel Process Technol.* 2005;86:1021-1053.
2. Bacon DW, Downie J, Hsu JC, Peters J. Modeling of fluidized bed gasifiers. In: Milne TA, Mudge KL, eds. *Fundamentals of Thermochemical Biomass Conversion*. London, UK: Elsevier Applied Science; 1985:717-732.
3. Double JM, Smith EL, Bridgwater AV. Computer modeling of fluidized bed gasifier. In: Ferrero GL, Maniatis K, Buekens A, eds. *Process and Gasification*. London, UK: Elsevier Applied Science; 1989:651-655.
4. Ruggiero M, Manfrida G. An equilibrium model for biomass gasification process. *Renewable Energy.* 1999;16:1106-1109.
5. Mansaray KG, Al-Taweel AM, Ghaly AE, Hamdullahpur F, Ugursal VI. Mathematical modeling of a fluidized bed rice husk gasifier: Part I—Model development. *Energy Sources.* 2000;22:83-98.
6. Altafini CR, Wamder PR, Barreto RM. Prediction of working parameters of a wood waste gasifier through an equilibrium model. *Energy Conv Manage.* 2003;44:2763–2777.
7. Li X, Grace JR, Lim CJ, Watkinson AP, Chen HP, Kim JR. Biomass gasification in a circulating fluidized bed. *Biomass Bioenergy.* 2004; 26:171-193.
8. De Souza-Santos ML. Comprehensive modeling and simulation of fluidized bed boilers and gasifiers. *Fuel.* 1989;68:1507-1521.
9. Hamel S, Wolfgang K. Mathematical modeling and simulation of bubbling fluidized bed gasifiers. *Powder Technol.* 2001;120:105-112.
10. Fiaschi D, Michelini M. A two-phase one-dimensional biomass gasification kinetic model. *Biomass Bioenergy.* 2001;21:121-132.
11. Bilodeau JF, Thérien N, Proulx P, Czernik S, Chornet E. A mathematical model of fluidized bed biomass gasification. *Can J Chem Eng.* 1993;71:549-557.
12. Sadaka SS, Ghaly AE, Sabbah MA. Two phase biomass air-steam gasification model for fluidized bed reactors: Part I—Model development. *Biomass Bioenergy.* 2002;22:439-462.
13. Radmanesh R, Mabrouk R, Chaouki J, Guy C. The effect of temperature on solids mixing in a bubbling fluidized bed reactor. *Int J Chem React Eng*. 2005a;3:A16 (http://www.bepress.com/ijcre/vol3/A16/)
14. Radmanesh R, Chaouki J, Guy C. A unified lumped approach in kinetic modeling of biomass pyrolysis. *Fuel.* 2006;85:1211-1220.
15. Nunn TR, Howard JB, Longwell JP, Peters WA. Product compositions and kinetics in the rapid pyrolysis of sweet gum hardwood. *Ind Eng Chem Process Des Dev.* 1985;24:836-844.
16. Van Deemter JJ. The countercurrent flow model of a gas–solids fluidized bed. In: *Proceedings of the International Symposium on Fluidization*. Amsterdam: Netherlands Univ. Press; 1967.
17. Radmanesh R, Chaouki J, Guy C. Modeling biomass pyrolysis in a bubbling fluidized bed reactor. Proceedings of the 7th World Congress of Chemical Engineering—Sustainable and Clean Technologies: Alternative Feeds, Glasgow, Scotland, July; 2005b.
18. Kunii D, Levenspiel O. *Fluidization Engineering* (Series in Chemical Engineering). 2nd Edition. Stoneham, MA: Butterworth-Heinemann; 1991.
19. Pyle DL, Zaror CA. Heat transfer and kinetics in the low temperature pyrolysis of solids. *Chem Eng Sci.* 1984;39:147-158.
20. Kersten SRA, Wang X, Prins W, van Swaaij WPM. Biomass pyrolysis in a fluidized bed reactor. Part 1: Literature review and model simulations. *Ind Eng Chem Res.* 2005;44:8773-8785.
21. Linjewile TM. *Temperature of Burning Carbonaceous Particles in a Fluidized Bed Combustor*. PhD Thesis. Adelaide, Australia: The Univ. of Adelaide; 1993.
22. Koufopanous CA, Papayannakos N, Maschio G, Lucchesi A. Modeling of pyrolysis of biomass particles. Studies on kinetic, thermal and heat transfer effects. *Can J Chem Eng.* 1991;69:907.
23. Di Blasi C. Modeling wood gasification in a countercurrent fixed-bed reactor. *AIChE J.* 2004;50:2306-2319.
24. Babu BV, Chaurasia AS. Dominant design variables in pyrolysis of

biomass particles of different geometries in thermally thick regime. *Chem Eng Sci.* 2004;59:611-622.
25. Bilbao R, Arauzo J, Salvador ML. Kinetics and modeling of gas formation in the thermal decomposition of powdery cellulose and pine sawdust. *Ind Eng Chem Res.* 1995;34:786-793.
26. González JF, Encinar JM, Canito JL, Sabio E, Chacon M. Pyrolysis of cherry stones: Energy uses of the different fractions and kinetic study. *J Anal Appl Pyrol.* 2003;67:165-190.
27. Hajaligol MR, Howard JB, Longwell JP, Peters WA. Product compositions and kinetics for rapid pyrolysis of cellulose. *Ind Eng Chem Process Des Dev.* 1982;21:457-465.
28. Boroson ML, Howard JB, Longwell JP, Peters WA. Product yields and kinetics from the vapor phase cracking of wood pyrolysis tars. *AIChE J.* 1989;35:120-128.
29. Roth J, Steiner G, Wolfinger MG, Staudinger G. Tar cracking from fast pyrolysis of large beech wood particles. *J Anal Appl Pyrol.* 2002;62: 83-92.
30. Wurzenberger JC, Wallner S, Raupenstrauch H, Khinast JG. Thermal conversion of biomass: Comprehensive reactor and particle modeling. *AIChE J.* 2002;48:2398-2411.
31. Bryden KM, Ragland K. Numerical modeling of deep fixed bed combustor. *Energy Fuel.* 1996;10:269.
32. Biba V, Macak J, Klose E, Malecha J. Mathematical modeling for the gasification of coal under pressure. *Ind Eng Chem Process Des Dev.* 1978;17:92-98.
33. Grace JR. In: Hetsroni G, ed. *Handbook of Multiphase Systems*. Washington, DC: Hemisphere; 1982:8-1.
34. Davidson JF, Harrison D. *Fluidized Particles*. New York: Cambridge Univ. Press; 1963.
35. Hoffmann AC, Janssen PBM, Prins J. Particle segregation in fluidized binary mixtures. *Chem Eng Sci*. 1993;48:1583-1592.
36. Kocatulum B, Basesme EA, Levy EK, Kozangolu B. Particle motion in the wake of a bubble in a gas-fluidized bed. Proceedings of the Annual Meeting of the American Institute of Chemical Engineers, Nov. 17–22, Los Angeles, CA; 1991:40-50.
37. Yates JG. *Fundamentals of Fluidized-Bed Chemical Processes*. London: Butterworths; 1983.
38. Corella J, Herguido J, Alday FJ. Pyrolysis and steam gasification of biomass in fluidized beds: Influence of the type and location of the biomass feeding point on the product distribution. In: Bridgwater AV, Kuester JL, eds. *Research in Thermochemical Biomass Conversion*. London, UK: Elsevier Applied Science; 1988:384.
39. Vriesman P, Heginuz E, Sjostrom K. Biomass gasification laboratory-scale AFBG: Influence of the location of the feeding pint on the fuel-N conversion. *Fuel.* 2000;79:1371-1378.
40. Narvaez I, Orio A, Aznar MP, Corella J. Biomass gasification with air in an atmospheric bubbling fluidized bed. Effect of six operational variables on the quality of the produced raw gas. *Ind Eng Chem Res.* 1996;35:2110-2120.
41. Gil J, Corella J, Aznar MP, Caballero MA. Biomass gasification in atmospheric and bubbling fluidized bed: Effect of the type of gasification agent on the product distribution. *Biomass Bioenergy.* 1999;17: 389-403.
42. Corella J, Aznar MP, Delgado J, Aldea E. Steam gasification of cellulosic wastes in a fluidized bed with downstream vessels. *Ind Eng Chem Res.* 1991;30:2252-2262.
43. Herguido J, Corella J, Gonzalez-saiz J. Steam gasification of lignocellulosic residues in a fluidized bed at a small pilot scale. Effect of the type of the feedstock. *Ind Eng Chem Res.* 1992;31:1274-1282.

Manuscript received Feb. 1, 2006, and revision received Aug. 21, 2006.